Selective Oxidation and Reactive Wetting During Hot-Dip Galvanizing of a 1.0 pct Al-0.5 pct Si TRIP-Assisted Steel

E.M. BELLHOUSE and J.R. McDERMID

Selective oxidation and reactive wetting during continuous galvanizing were studied for a low-alloy transformation induced plasticity (TRIP)-assisted steel with 0.2 pct C, 1.5 pct Mn, 1.0 pct Al and 0.5 pct Si. Three process atmospheres were tested during annealing prior to galvanizing: 220 K (–53 °C) dew point (dp) N_2-20 pct H_2, 243 K (–30 °C) dp N_2-5 pct H_2 and 278 K (+5 °C) dp N_2-5 pct H_2. The process atmosphere oxygen partial pressure affected the oxide chemistry, morphology and thickness. For the 220 K (–53 °C) dp and 243 K (–30 °C) dp process atmospheres, film and nodule-type manganese, silicon and aluminum containing oxides were observed at the surface. For the 278 K (+5 °C) dp atmosphere, MnO was observed at the grain boundaries and as thicker localized surface films. Oxide morphology, thickness and chemistry affected reactive wetting, with complete wetting being observed for the 220 K (–53 °C) dp and 243 K (–30 °C) dp process atmospheres and incomplete reactive wetting being observed for the 278 K (+5 °C) dp atmosphere. Complete reactive wetting for the 220 K (–53 °C) dp and 243 K (–30 °C) dp process atmospheres was attributed to a combination of zinc bridging of oxides, aluminothermic reduction of surface oxides and wetting of the oxides. Incomplete wetting for the 278 K (+5 °C) dp atmosphere was attributed to localized thick MnO films.

I. INTRODUCTION

IN the automotive industry, there is a continuing demand for improved safety and decreased vehicle weight. Low alloy transformation induced plasticity (TRIP)-assisted steels can satisfy these demands through their high strength and ductility, allowing thinner cross sections of material to be used while providing excellent energy absorption in the event of a collision.[1–3] These mechanical properties are brought about by the TRIP steel microstructure, which consists of ferrite, bainitic ferrite, retained austenite that transforms to martensite during deformation (*i.e.*, the TRIP effect) and occasionally a small amount of athermal martensite.[4,5] The TRIP effect is of particular importance as it provides strengthening by two mechanisms: (1) dynamic composite strengthening through the appearance of stronger martensite particles in the microstructure during deformation and (2) increased work hardening of ferrite by dislocations introduced to accommodate the volume expansion associated with the austenite to martensite transformation.[6,7] To be used in automotive exposed parts, corrosion protection of TRIP steels is essential to maintain structural integrity of the part and satisfy consumer durability expectations. The continuous galvanizing process is amongst the most cost effective methods of achieving this objective. However, the galvanizing of TRIP steels poses some unique challenges. For example, the thermal cycle required to obtain optimal TRIP steel microstructures and mechanical properties is not necessarily compatible with continuous hot-dip galvanizing. Also, selective oxidation of the alloying elements commonly used in TRIP steels can result in incomplete reactive wetting, causing bare spot defects in the zinc coating.

TRIP steels require a specialized heat treatment which includes intercritical annealing (IA) and an isothermal bainitic transformation (IBT) in order to obtain the desired TRIP steel microstructure and mechanical properties. This two stage heat treatment is not necessarily compatible with continuous hot-dip galvanizing as the IBT stage of the heat treatment is generally carried out in the temperature range of 633 K (360 °C) to 723 K (450 °C),[4–14] whereas the molten Zn (Al, Fe) bath is generally held at 733 K (460 °C) and the steel strip is usually held slightly above this temperature prior to entering the zinc bath. There is some concern about using higher IBT temperatures due to possible carbide precipitation,[15,16] and mechanical property degradation has been observed when using higher IBT temperatures.[15–18]

Despite these concerns some authors have successfully obtained excellent combinations of strength and ductility using thermal cycles having IBT temperatures of 733 K (460 °C) to 743 K (470 °C).[16,19–22] The microstructure and mechanical properties of the steel used in the present work were previously investigated using a thermal cycle with an IBT temperature of 738 K (465 °C). The best combination of strength and ductility obtained for the present steel was an ultimate tensile strength of 1009 MPa and uniform elongation of 0.22

E.M. BELLHOUSE, formerly Doctoral Student, with the McMaster Steel Research Centre, McMaster University, 1280 Main St. W., JHE 357, Hamilton, ON L8S 4L7, Canada, is now a Researcher with the New Sheet Product/Coating Development, ArecelorMittal Dofasco, Box 2460, 1330 Burlington St. E., Hamilton, ON L8N 3J5, Canada. J.R. McDERMID, Professor, is with the McMaster Steel Research Centre, McMaster University. Contact e-mail: mcdermid@mcmaster.ca

(true stress–true strain); the thermal cycle which resulted in these properties was used in the present investigation.[22]

The other problem encountered when galvanizing TRIP steels is that selective oxidation of the alloying elements manganese, silicon and/or aluminum can prevent the Zn (Al, Fe) bath from reactively wetting the substrate, resulting in bare spot defects and unacceptable coatings.[23–28] Silicon, in particular, has been shown to cause incomplete reactive wetting[26,28] with improved wetting results obtained when replacing silicon in the steel chemistry with aluminum or phosphorus.[24,27,28] Silicon, however, is desirable in the steel chemistry as it provides significant solid solution strengthening and delays carbide precipitation from austenite during the IBT.[9,29]

With manganese, aluminum and silicon in the steel chemistry there are a number of different oxides which can form according to the MnO-Al_2O_3-SiO_2 phase diagram as defined by Jung et al.[30,31] As well as MnO, Al_2O_3 and SiO_2 it is possible for more complex oxides to form, including Mn_2SiO_4, $MnSiO_3$, $MnAl_2O_4$, $Al_6Si_2O_{13}$, $Mn_2Al_4Si_5O_{19}$ and $Mn_3Al_2Si_3O_{12}$. Experimentally, the selective oxidation of TRIP steels with silicon partially replaced by aluminum has been investigated by TEM.[32,33] Gong et al.[32] studied a TRIP steel containing 0.158 pct C, 1.99 pct Mn, 1.01 pct Al and 0.31 pct Si using a 248 K (–25 °C) dp N_2-10 pct H_2 process atmosphere. The oxides found on the surface had a range of compositions and were identified as $xMnO\cdot SiO_2$ ($1 \leq x \leq 4$) and $xMnO\cdot Al_2O_3$ ($x \geq 1$), where the oxide morphology comprised films and nodules. Oxides were also observed as precipitates below the steel surface. Li et al.[33] studied a steel containing 0.15 pct C, 1.55 pct Mn, 1.51 pct Al, 0.29 pct Si and 0.51 pct Cu, using a 238 K (–35 °C) dp N_2-5 pct H_2 process atmosphere. $MnAl_2O_4$ was identified as well as an unidentified silicon containing amorphous oxide.[33] Galvanizing of a TRIP steel with 0.31 pct C, 1.57 pct Mn, 1.23 pct Al and 0.34 pct Si was studied by Mahieu et al.[24] Complete reactive wetting was obtained for this steel using a 243 K (–30 °C) dp N_2-5 pct H_2 process atmosphere and was attributed to the absence of silicon containing oxides at the surface, despite having 0.34 pct Si in the steel chemistry. Only manganese and aluminum oxidation was detected at the surface. The results of Mahieu et al.[24] contradict the results of Gong et al.[32] and Li et al.,[33] who observed silicon containing oxides after annealing aluminum containing TRIP steels having 0.31 pct Si and 0.29 pct Si, respectively, using a similar process atmosphere.

The oxidation and galvanizing of a series of Al-Si TRIP-assisted steels containing 0.2 pct C and 1.5 pct Mn, where the sum of the Si and Al concentrations was equal to 1.5 pct, have been studied by the present authors.[34,35] This work has emphasized the relationship between oxide chemistry and morphology on reactive wetting by the Zn (Al, Fe) bath. It was determined that for the 1.5 pct Si and 1.0 pct Si + 0.5 pct Al TRIP steels, oxide morphology was the most important factor for determining reactive wetting behavior with small, closely spaced manganese and silicon rich oxide nodules resulting in incomplete reactive wetting for a 278 K

(+5 °C) dp N_2 -5 pct H_2 process atmosphere.[34] For the steel with 1.5 pct Al and very low Si, it was determined that oxide thickness was the most important factor in determining the reactive wetting behavior, with thicker localized MnO films resulting in an increased number of bare spots in the zinc coating when using a 278 K (+5 °C) dp N_2-5 pct H_2 process atmosphere.[35] All steels studied exhibited complete reactive wetting when employing either a 220 K (–53 °C) dp N_2-20 pct H_2, a 223 K (–50 °C) dp N_2-20 pct H_2, or a 243 K (–30 °C) dp N_2-5 pct H_2 process atmosphere.[34,35]

The relationship between oxide chemistry, morphology and reactive wetting is an area for which sparse literature can be found in the area of continuous galvanizing. The objectives of the present work are to study the surface chemistry, oxide morphology and mechanism of reactive wetting during galvanizing of a 0.2 pct C, 1.5 pct Mn, 1.0 pct Al and 0.5 pct Si TRIP-assisted steel.

II. EXPERIMENTAL METHOD

The chemical composition of the experimental TRIP steel is shown in Table I. The steel was cast, hot rolled to a thickness of 4 mm, sandblasted, pickled and cold rolled to a thickness of approximately 1.5 mm. The hot rolling start and finish temperatures were 1523 K (1250 °C) and 1123 K (850 °C), respectively. Experimental steel panels were 120 mm × 200 mm with the longitudinal axis parallel to the rolling and dipping directions. A uniform temperature and coating area of 90 mm × 90 mm was centered on the lower portion of the panels and only material from this area was analyzed. Prior to heat treatment the panels were degreased in a solution of 2 pct NaOH heated to 353 K (80 °C), rinsed with water, cleaned with isopropanol in an ultrasonic bath and dried with warm air. A final cleaning with acetone was performed immediately prior to the samples entering the galvanizing simulator.

All annealing and galvanizing experiments were performed in the McMaster Galvanizing Simulator (MGS) (Iwatani Surtec, Dusseldorf, Germany). The MGS consists of an atmosphere controlled column comprising a number of sections (Figure 1). At the top is a sample loading and cooling section. Sample cooling was performed using two parallel gas platens. Below this section is the heating section which comprises a quartz lamp infrared furnace and a high frequency induction furnace; only the former was used in the present work as the latter is used for galvannealing. The upper sections of the MGS are separated from the zinc pot and gas-jet wiping knives by an airlock, where the zinc pot consists of a resistance heated 50 kg graphite crucible controlled

Table I. Chemical Composition of Experimental TRIP Steel (Weight Percent)

Alloy Name	C	Mn	Si	Al	Ti
1.0 pct Al steel	0.20	1.52	0.45	1.0	0.021

to within ±2 K using a conventional process controller. The zinc bath temperature was 733 K (460 °C), contained 0.2 pct dissolved Al and was Fe saturated.[36] Immediately above the zinc bath are gas jet wiping knives, which control the coating thickness using a 500 L/min N_2 gas flow to yield a coating weight of 70 g/m^2/side. The sample heating and cooling cycle was controlled using a 0.5 mm type K thermocouple welded directly to the sample.

The thermal cycle consisted of heating at +10 K/s to the IA temperature of 1098 K (825 °C), holding at 1098 K for 120 seconds, cooling at –20 K/s to the IBT temperature of 738 K (465 °C) and holding at this temperature for 120 seconds, followed by rapid cooling to room temperature. The IA temperature was chosen to produce an intercritical microstructure of 50 pct ferrite (α)-50 pct austenite (γ) (vol pct) as determined using THERMO-CALC* software and the TCFE2 database.

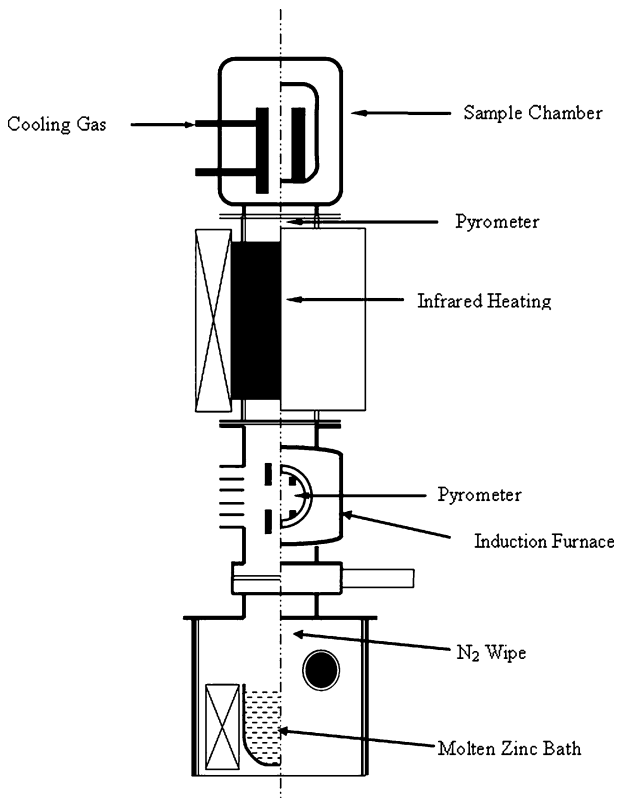*THERMO-CALC is a trademark of Thermo-Calc, Stockholm.

Fig. 1—Schematic drawing of the MGS.

Samples that were galvanized were dipped in the Zn (Al, Fe) bath for 4 seconds following 116 seconds of the IBT.

Three process atmospheres were tested to determine the effect of oxygen partial pressure on selective oxidation and reactive wetting (Table II). Process atmospheres and their attendant samples will be distinguished by their dew point in the subsequent text. The oxygen partial pressure listed in Table II was calculated at the IA temperature of 1098 K (825 °C) using the thermodynamic data of Fine and Geiger.[37]

Selected samples were subjected to the thermal cycle without dipping in the Zn (Al, Fe) bath in order to study the effect of process atmosphere oxygen partial pressure on the surface chemistry and oxide morphology. For these experiments, it was necessary to polish the sample surface to eliminate the effect of roughness on subsequent analyses. Samples analyzed using X-ray photoelectron spectroscopy (XPS) were polished using 4000 grit SiC paper prior to annealing. For samples analyzed with scanning Auger microscopy (SAM) and transmission electron microscopy (TEM), the surface was polished using 0.05 μm alumina. For all oxidation experiments the samples were stored in anhydrous isopropanol immediately after removal from the MGS to minimize further surface oxidation prior to analysis with XPS, SAM or TEM.

Chemical analysis of the steel surface and compositional depth profiles were obtained using XPS. XPS was performed using a PHI Quantera X-ray photoelectron spectroscope (Physical Electronics, Chanhassen, MN) with an Al K_α X-ray source. The spot size was 100 μm and the take off angle was 45 deg. The accuracy of the chemical composition measurements were ±5 pct of the measured value in atomic percent for each element. XPS depth profiles were obtained by argon sputtering followed by analysis of the new surface. The accuracy of the sputtering depth was ±10 pct of the indicated depth. Surface oxides were identified from the measured binding energy after sputtering to a depth of 5 nm. The binding energy values obtained were accurate to within ±0.1 eV and all spectra were calibrated using the metallic iron binding energy of 706.62 eV.

The relationship between steel surface oxide morphology and elemental distribution was determined using SAM elemental mapping. SAM data was collected using a JEOL** JAMP-9500F field emission Auger

---

**JEOL is a trademark of Japan Electron Optics Ltd., Tokyo.

---

microprobe. The energy of the primary electron beam was 15 keV. Samples were tilted 30 deg towards the

Table II. Experimental Annealing Atmospheres

Atmosphere Name	Dew Point (K (°C))	N_2 Content (Vol Pct)	H_2 Content (Vol Pct)	pO_2 at 1098 K (825 °C), Atm
220 K (–53 °C) dp	220 (–53)	80	20	8.60E-26
243 K (–30 °C) dp	243 (–30)	95	5	1.68E-22
278 K (+5 °C) dp	278 (+5)	95	5	4.75E-20

electron analyzer. Auto probe tracking was in effect during the collection of elemental maps to compensate for sample drift. The signal intensity (I) was calculated using Eq. [1] to attenuate the effect of topography.

$$I = \frac{\text{peak} - \text{background}}{\text{background}} \quad [1]$$

Elemental maps were collected from the as-annealed steel surface and after argon sputtering for one minute, equivalent to a depth of 20 nm, to eliminate surface contaminants originating from storage. The accuracy of the sputtering depth was ±10 pct. With the exception of the oxygen map, elemental maps were very similar before and after sputtering. Prior to sputtering, it should be noted that iron was oxidized, an artifact of sample atmospheric exposure following removal from the MGS. Due to the similarities observed before and after sputtering only elemental maps after sputtering are shown.

TEM was used to analyze cross-sections of oxidized and galvanized samples. TEM samples were made via focused ion beam (FIB) milling using a NVision 40 by Zeiss (Carl Zeiss, Oberkochen, Germany) to obtain a site-specific sample of either the oxidized surface or steel/coating interface. Oxidized samples were sputter coated with either gold or platinum to avoid sample charging. Carbon was deposited over the sample location prior to FIB milling to prevent preferential sputtering of either the oxide or zinc coating. TEM was performed with a JEOL 2010F TEM equipped with an Oxford INCA Pentafet (Oxford Instruments, Abingdon, Oxfordshire, UK) energy dispersive X-ray (EDX) spectrometer. The TEM acceleration voltage was 200 keV. EDX was performed in scanning transmission electron microscopy (STEM) mode with a probe size of 1 nm. The experimental error associated with the EDX measurements was within ±10 pct for all elements with the exception of oxygen and nitrogen where the error was significantly higher.

Reactive wetting was quantified by counting and measuring any bare spot coating defects within the uniform temperature and coating area. Two galvanized panels were analyzed for each process atmosphere. Image analysis of the bare spots on the galvanized panels was performed using a Carl Zeiss Ltd. (Carl Zeiss Canada Ltd., Toronto, ON, Canada). Stemi 2000-C stereoscope and Northern Eclipse Version 6.0 image analysis software by Empix Imaging Inc. (Mississauga, ON, Canada). Images were captured using a magnification of 5×. The bare spot area was measured by manually selecting the bare spot perimeter. The measured bare spot area is accurate to within ±0.01 mm^2.

Scanning electron microscopy (SEM) was used to analyze the interfacial reaction products at the steel/coating interface. To expose the interfacial reaction products, the zinc overlay was stripped using two methods: (1) fuming nitric acid (HNO$_3$) and (2) 10 vol pct sulfuric acid (H$_2$SO$_4$) in water. Fuming nitric acid also strips any Fe-Zn intermetallics present at the steel/coating interface, whereas the 10 pct H$_2$SO$_4$ solution leaves any Fe-Zn intermetallics intact. SEM was performed using a JEOL 7000F field emission scanning electron microscope. The acceleration voltage was

10 keV for the 220 K (–53 °C) dp and 243 (–30 °C) dp samples and was 5 keV for the 278 K (+5 °C) dp samples.

III. RESULTS

A. *Selective Oxidation*

The chemical composition of the steel surface as determined by XPS is shown in Figure 2. For the 220 K (–53 °C) dp process atmosphere the surface was almost completely covered by alloying element oxides, as shown by the low iron concentration of the steel surface (4.7 at. pct). As the oxygen partial pressure of the process atmosphere increased the concentration of iron at the surface increased. The silicon and aluminum concentrations at the surface were highest for the 220 K (–53 °C) dp atmosphere and decreased as the process atmosphere oxygen partial pressure increased. The maximum manganese concentration at the surface was observed for the 243 K (–30 °C) dp process atmosphere.

XPS depth profiles were obtained to investigate the oxide thickness and determine the subsurface behavior of the alloying elements (Figure 3). It was observed that the surface and subsurface enrichment of aluminum was different than that of manganese and silicon. The manganese and silicon enrichments were higher at the surface and their concentrations decreased with increasing depth into the steel surface. After an initial decrease in aluminum concentration, there was an increase in aluminum concentration starting at approximately 100 nm below the steel surface, as can be seen clearly for the 220 K (–53 °C) dp and 243 K (–30 °C) dp process atmospheres (Figures 3(a) and (b)).

XPS binding energy data was used to identify the surface oxides. In the case of the 220 K (–53 °C) dp and 243 K (–30 °C) dp process atmospheres the oxides could not be unambiguously identified as Mn, Al and Si
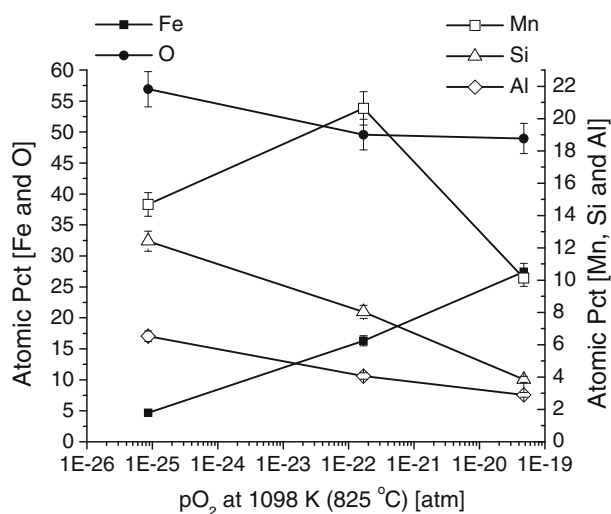
Fig. 2—Chemical composition of the steel surface as a function of process atmosphere oxygen partial pressure as determined by XPS (after sputtering 5 nm).

enrichments often occurred together, as will be shown in the SAM and TEM results. Furthermore, binding energy data for complex oxides such as $MnSiO_3$, $Mn_2Al_4Si_5O_{19}$ and $Mn_3Al_2Si_3O_{12}$ are not currently available. In the case of Mn, Figures 4(a) and (b) show Mn $2p_{3/2}$ XPS binding energy peaks corresponding to
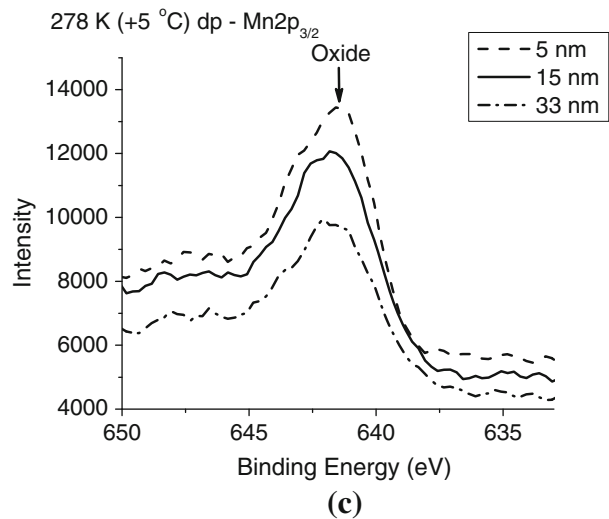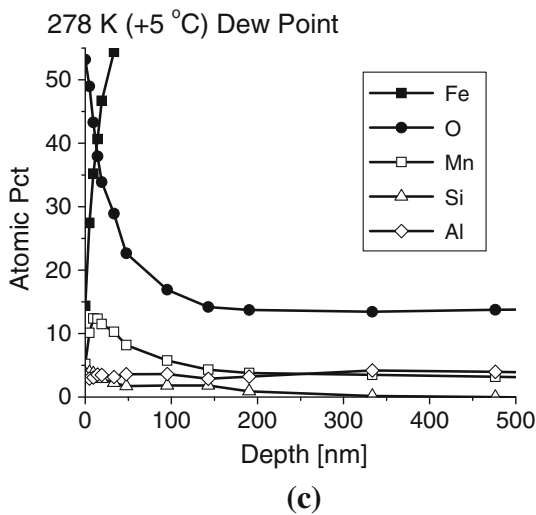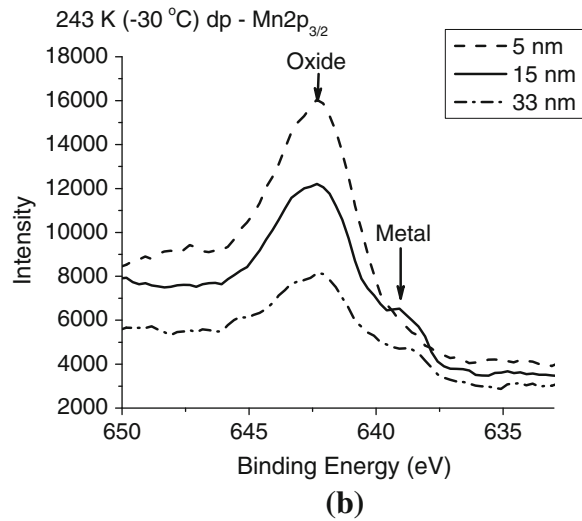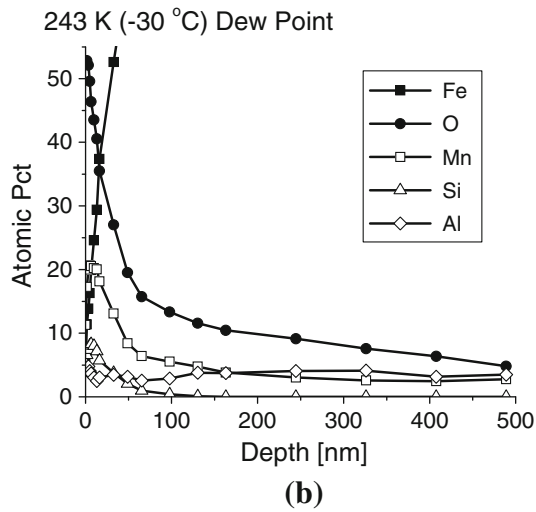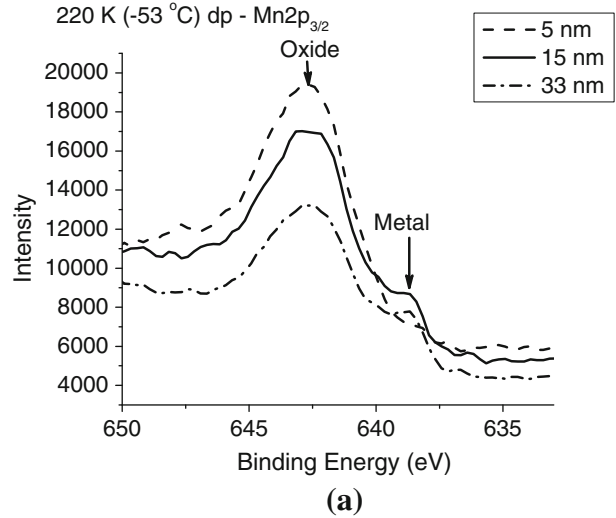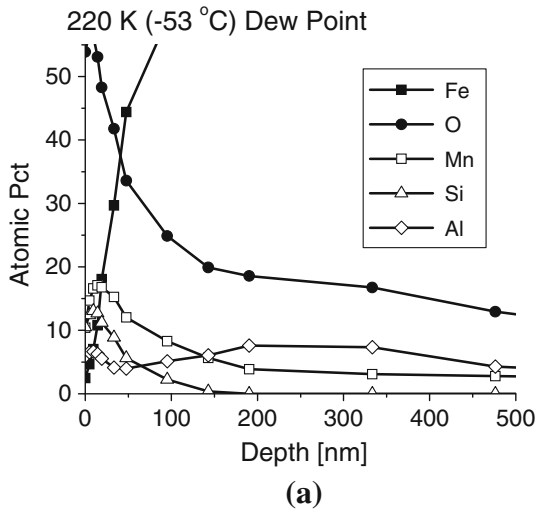

Fig. 3—XPS depth profiles for the (a) 220 K (−53 °C) dp, (b) 243 K (−30 °C) dp and (c) 278 K (+5 °C) dp process atmospheres.

Fig. 4—Mn $2p_{3/2}$ XPS spectra for the (a) 220 K (−53 °C) dp, (b) 243 K (−30 °C) dp and (c) 278 K (+5 °C) dp.

oxidized Mn and Mn metal[38,39] observed for sputtering depths of 5, 15 and 33 nm. Enrichment of metallic Mn above the alloy bulk concentration (1.5 at. pct) was observed, with 3 and 3.7 at. pct Mn for the 220 K (–53 °C) dp steel and 3.6 and 2.6 at. pct Mn for the 243 K (–30 °C) dp steel at depths of 15 and 33 nm, respectively. For the 278 K (+5 °C) dp samples (Figure 4(c)), only MnO was identified for all sputtering depths.[38,39]

The relationship between oxide morphology and surface chemistry was determined by SAM and TEM. The SAM results for the 220 K (–53 °C) dp sample are shown in Figure 5 and the TEM results are shown in Figure 6 and Table III. The secondary electron image suggests that the oxide morphology was primarily film-type (Figure 5(a)). The SAM elemental map results show that the vast majority of the surface was covered in
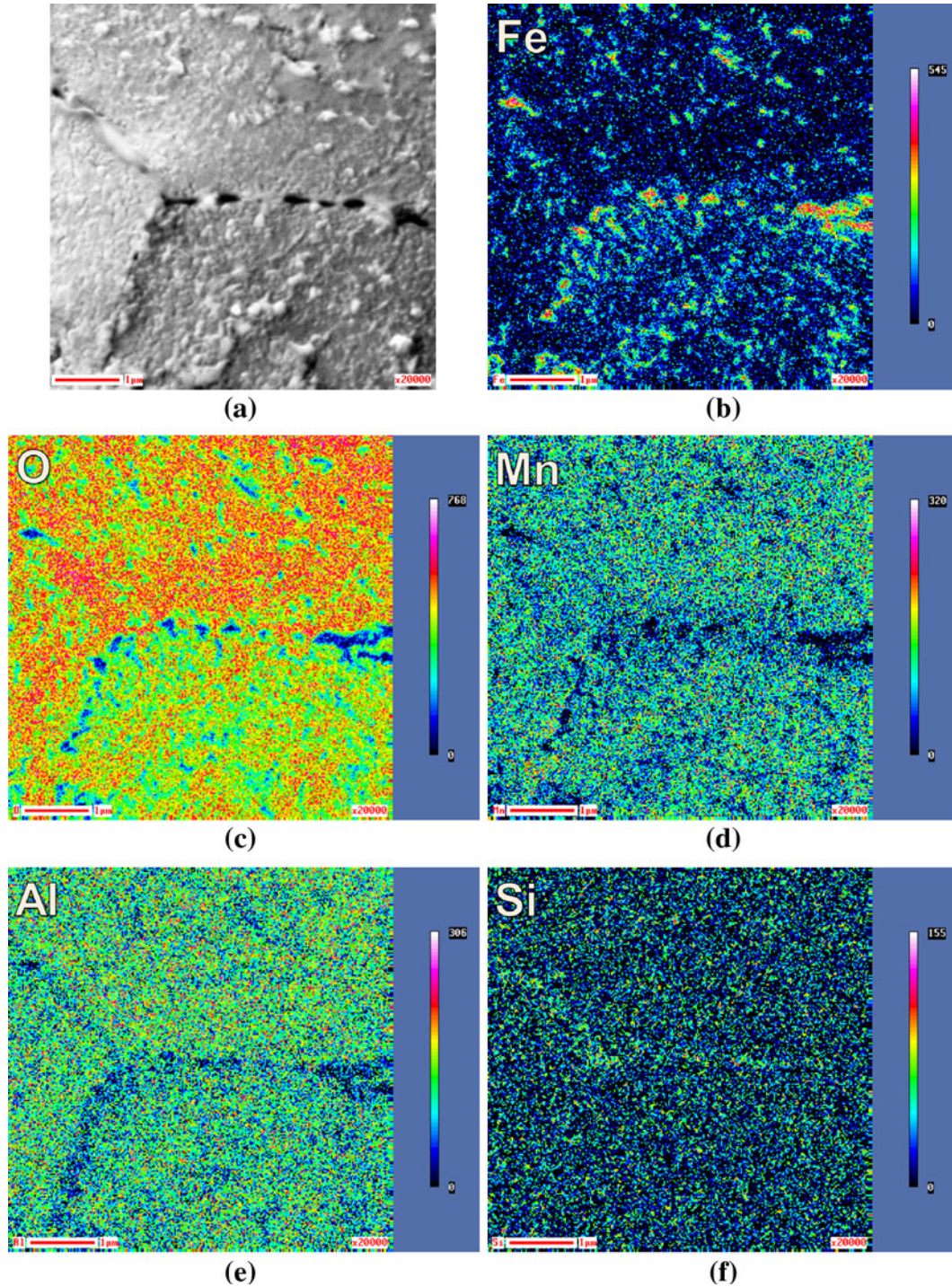

Fig. 5—Elemental mapping of the 220 K (–53 °C) dp steel with scanning Auger microscopy after sputtering 20 nm: (a) secondary electron image, (b) Fe, (c) O, (d) Mn, (e) Al and (f) Si.

Mn, Al and Si rich oxides (Figure 5). Only a small amount of iron was observed at the surface (Figure 5(b)), in agreement with the low iron surface concentrations as determined by XPS (Figures 2 and 3(a)). The silicon concentration was slightly higher at the grain boundaries (Figure 5(f)).

The results of the TEM study showed a mixture of film-type oxides and closely spaced nodules (Figure 6). The chemical composition of points A through D indicated in Figure 6 are shown in Table III. The black particles on the top surface are the gold coating. The composition of point A shows that the film-type oxide was rich in Si, Mn and Al (Table III). The film-type oxide was not continuous as shown by the gap in the oxide layer to the left of point A in Figure 6(a). The oxide films were 35 to 40 nm thick. Figure 6(b) shows a substrate grain boundary. Analysis of point B (Table III) showed that the oxide at this grain boundary had a higher Si content, consistent with the SAM results (Figure 5). As can be seen in Figure 6(c), the oxide nodules were separated by areas with either a thin oxide film (between points C and D) or no apparent oxide film (right of point D). These oxides had a range of chemical compositions; for example, points A and D were Si-rich and at point C the Mn and Al concentrations were both higher than the Si concentration.

The relationship between surface oxide morphology and elemental distribution for the 243 K (–30 °C) dp steel was determined using SAM and these results are shown in Figure 7. The secondary electron image in Figure 7(a) shows that there was a mixture of film and nodule-type oxides at the steel surface. These oxides were rich in Mn, Al and Si (Figures 7(d) through (f)). At the right of the area analyzed were regions having a higher concentration of Al and lower Mn concentration Figures 7(d) and (e)). The oxide morphology of the 243 K (–30 °C) dp steel was similar to the 220 K (–53 °C) dp steel, however, more iron was identified at the surface of the 243 K (–30 °C) dp steel in agreement with the XPS results (Figure 2). The region of the surface having a higher iron concentration (lower left) coincided with an area having small nodules, whereas the rest of the area analyzed had a film-type morphology.

SAM elemental maps for the 278 K (+5 °C) dp sample are shown in Figure 8. The Al and Si maps are not shown for this sample as no Al or Si rich features were observed. The lack of Al and Si observed at the surface by SAM agrees with the low concentrations of these elements observed by XPS (Figure 2). The Mn and O maps show that Mn oxidation was observed at the grain boundaries and as localized film-type oxides at the surface (Figures 8(c) and (d)). There was a larger amount of iron observed at the surface of the 278 K (+5 °C) dp steel when compared to the lower oxygen partial pressure process atmospheres (Figure 8(b)) in agreement with the
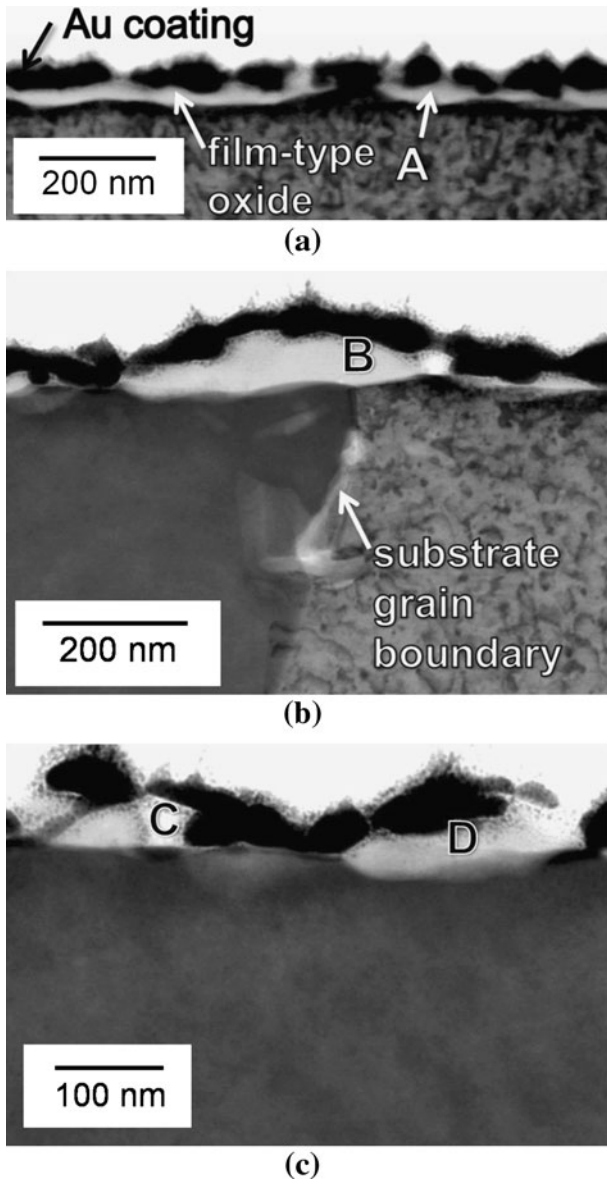

Fig. 6—STEM bright field images of the 220 K (–53 °C) dp steel: (a) film-type morphology, (b) substrate grain boundary and (c) shows nodule-type morphology. Analysis of points A through D is provided in Table III.

Table III. TEM EDX Analysis Corresponding to Points A Through E in Figs. 6 and 9 for the Oxidized 220 K (–53 °C) dp Steel and 278 K (+5 °C) dp Steel, Respectively (Atomic Percent)

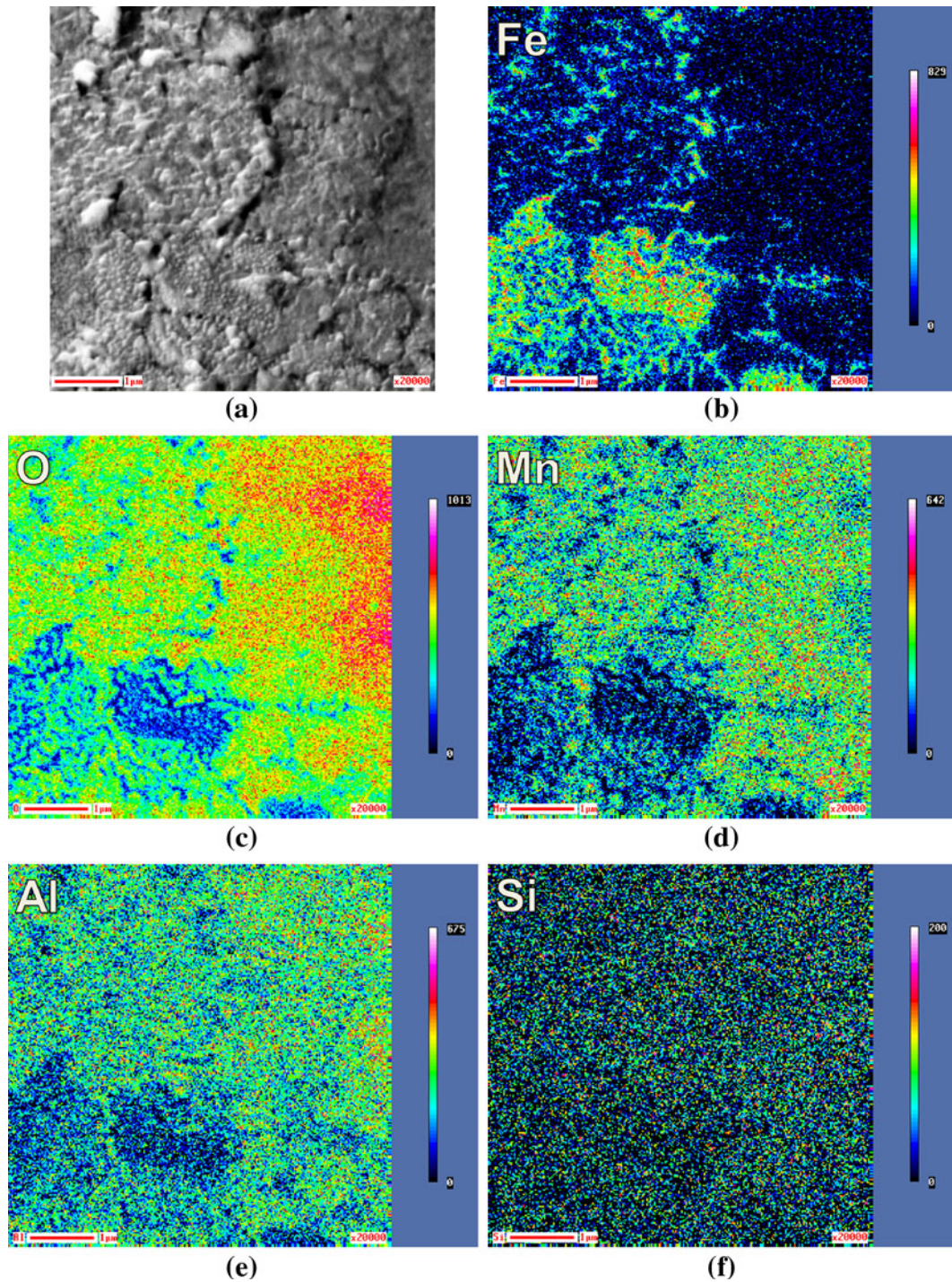| Figure	Point	Fe	O	Mn	Al	Si	Phase Present
6	A	6.1	46.2	14.5	9.8	23.4	Mn, Si and Al oxide
6	B	1.1	52.8	2.7	0.8	42.7	SiO_x ($x < 2$)
6	C	10.6	46.4	17.7	14.7	10.7	Mn, Si and Al oxide
6	D	2.1	49.8	16.3	10.2	21.6	Mn, Si and Al oxide
9	E	14.7	37.9	38.0	1.7	1.0	MnO

Fig. 7—Elemental mapping of the 243 K (–30 °C) dp steel with scanning Auger microscopy after sputtering 20 nm: (*a*) secondary electron image, (*b*) Fe, (*c*) O, (*d*) Mn, (*e*) Al and (*f*) Si.

higher Fe concentration at the surface observed by XPS at the 278 K (+5 °C) dp (Figure 2).

TEM analysis of the 278 K (+5 °C) dp steel is shown in Figure 9 and Table III. The localized manganese rich oxide film found by SAM was identified as MnO by EDX analysis (point E, Figure 9(a) and Table III), in agreement with the XPS binding energy analysis (Figure 4(c)). The thickness of the MnO film was determined to be 90 and 75 nm at the locations indicated in Figure 9(d).

Below the surface, internal oxidation of Mn, Si and Al was observed (Figure 9(c) through (f)).

B. *Reactive Wetting*

The degree of reactive wetting was determined by counting and measuring any bare spots in the zinc coating, identifying the interfacial reaction products by SEM and studying the cross-section of the galvanized
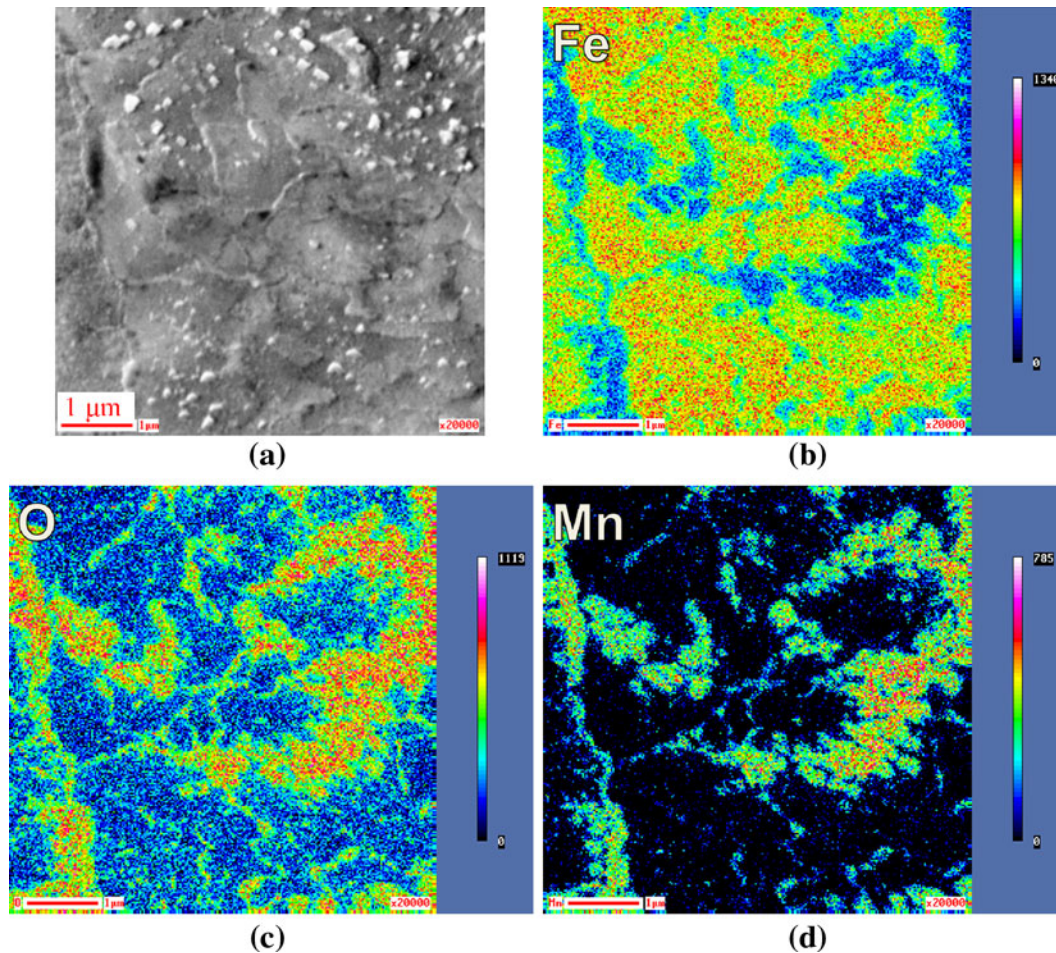
Fig. 8—Elemental mapping of the 278 K (+5 °C) dp steel with scanning Auger microscopy after sputtering 20 nm: (a) secondary electron image, (b) Fe, (c) O, and (d) Mn.

steel by TEM. The bare spot analysis is shown in Table IV. Complete reactive wetting was observed when using the 220 K (–53 °C) dp and 243 K (–30 °C) dp process atmospheres with few bare spots and a small total percent bare area. There was an increase in the number of bare spots and percent bare area (*i.e.*, incomplete reactive wetting) when using the 278 K (+5 °C) dp process atmosphere.

The interfacial reaction products were identified by their well-known morphologies using SEM.[40–42] $Fe_2Al_5Zn_x$ and $FeZn_{13}$ were identified at the steel/coating interface for all process atmospheres (Figure 10). The $Fe_2Al_5Zn_x$ layer was found to be continuous for the 220 K (–53 °C) dp process atmosphere (Figure 10(a)) whereas for the 243 K (–30 °C) dp and 278 K (+5 °C) dp atmospheres the $Fe_2Al_5Zn_x$ layer was not continuous (Figures 10(c) and (e)), indicating that some inhibition breakdown had occurred.

TEM EDX mapping across the steel/coating interface for the 220 K (–53 °C) dp steel is shown in Figure 11, and EDX point analyses of points A through F are shown in Table V. Two different areas are shown as a result of the variety of information obtained from this sample. Selected elemental maps are overlaid in color to show the relationship between oxides and the $Fe_2Al_5Zn_x$

layer. In Figures 11(a) through (c), the Mn map is shown in red and the Al map is shown in green; in Figure 11(c), the Fe map is shown in blue. Aluminum rich needle like precipitates, likely AlN, were identified below the steel surface (Figure 11(a) and Table V, point A). The formation of AlN during annealing of Al containing steels in N_2 rich atmospheres has been observed previously.[28,32,33,35] Analysis of point B shows Al_2O_3 at a grain boundary below the steel surface. At the steel/coating interface in Figure 11(a), two $Fe_2Al_5Zn_x$ morphologies relative to the oxides remaining at the interface after galvanizing were observed. As can be seen by comparing the Mn and Al maps, in the upper portion of Figure 11(a), $Fe_2Al_5Zn_x$ formed between larger Mn-rich particles and in the lower portion of Figure 11(a) a thicker $Fe_2Al_5Zn_x$ layer formed above smaller Mn-rich particles. This area of the steel/coating interface is shown at higher magnification in Figure 11(b). EDX analysis of point C identified the larger nodules as Mn-rich (Mn, Si, Al) oxides (Table V). $Fe_2Al_5Zn_x$ was found between these oxide particles as shown by the analysis of point D (Figure 11(b)) in Table V. Figure 11(c) shows an area where wetting of an oxide film (point F, Table V) was observed. A continuous $Fe_2Al_5Zn_x$ layer was observed over this film as
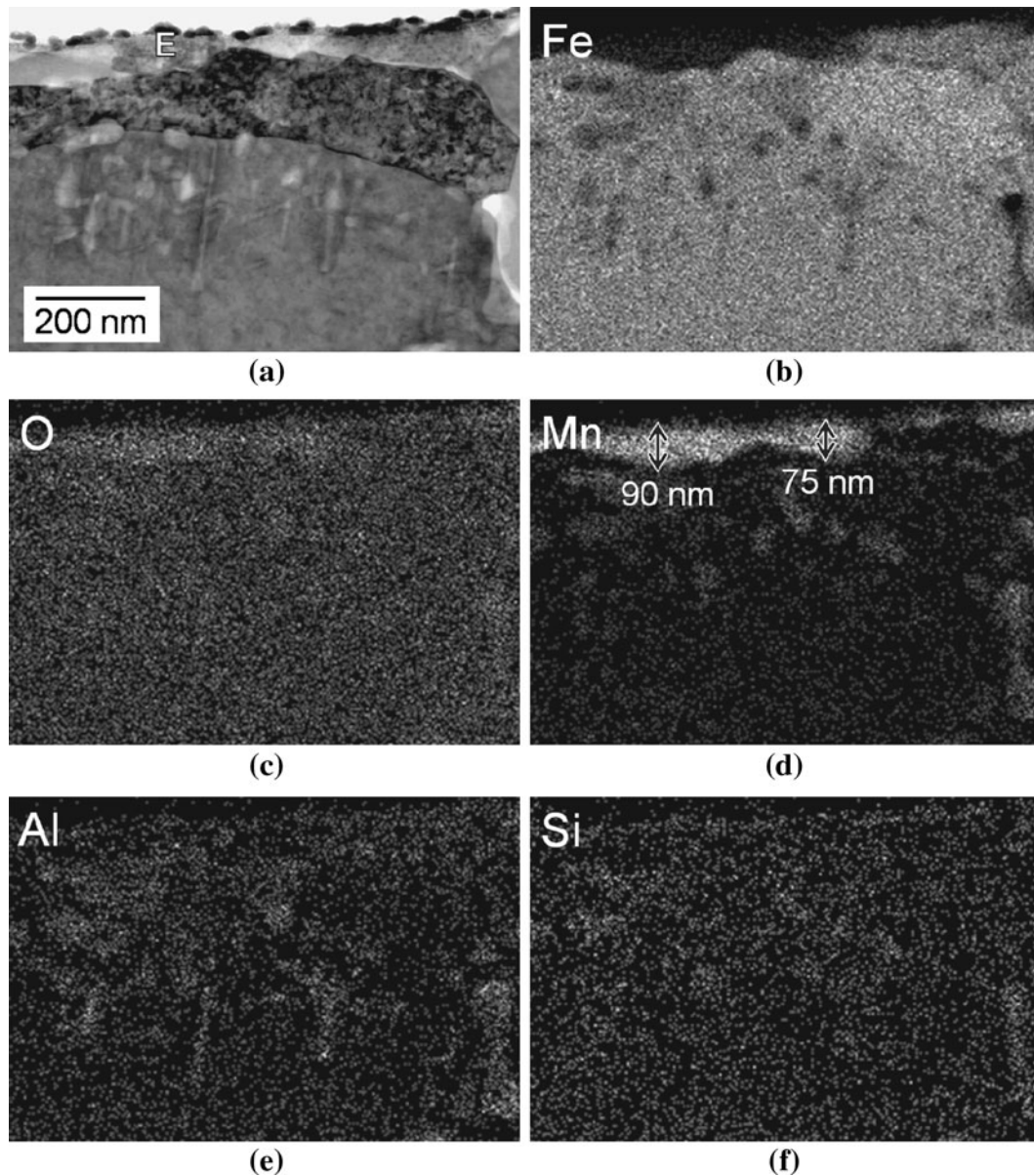
Fig. 9—TEM EDX elemental mapping of the 278 K (+5 °C) dp steel: (a) STEM bright-field image, (b) Fe, (c) O, (d) Mn, (e) Al and (f) Si maps. Analysis of point E is provided in Table III.

Table IV. Bare Spot Analysis (Average of Two Panels)

Sample Name	Number of Bare Spots/Panel	Total Bare Area/Panel* (mm^2)	Pct Bare Area
220 K (−53 °C) dp	7	1.17	0.014
243 K (−30 °C) dp	5	2.98	0.037
278 K (+5 °C) dp	49	26.47	0.33

*The area analyzed on each panel was 8100 mm^2.

shown by the Al map (Figure 11(c)) and by the analysis of point E (Table V).

A cross-section of a galvanized 278 K (+5 °C) dp sample was analyzed by TEM at the edge of a bare spot in the zinc overlay. To the left of the area shown in Figure 12, reactive wetting was observed with an integral $Fe_2Al_5Zn_x$ layer. Within the bare spot a thick MnO layer was present, as shown by the EDX analysis of point H in Table V. Thickness measurements for this nonwetted MnO are indicated on the Mn map in Figure 12(b), which showed that this oxide thickness reached approximately 160 nm.

IV. DISCUSSION

A. *Selective Oxidation*

Selective oxidation of the steel surface was studied by XPS, SAM and TEM. XPS and SAM showed that with increasing process atmosphere oxygen partial pressure the iron concentration at the steel surface increased and
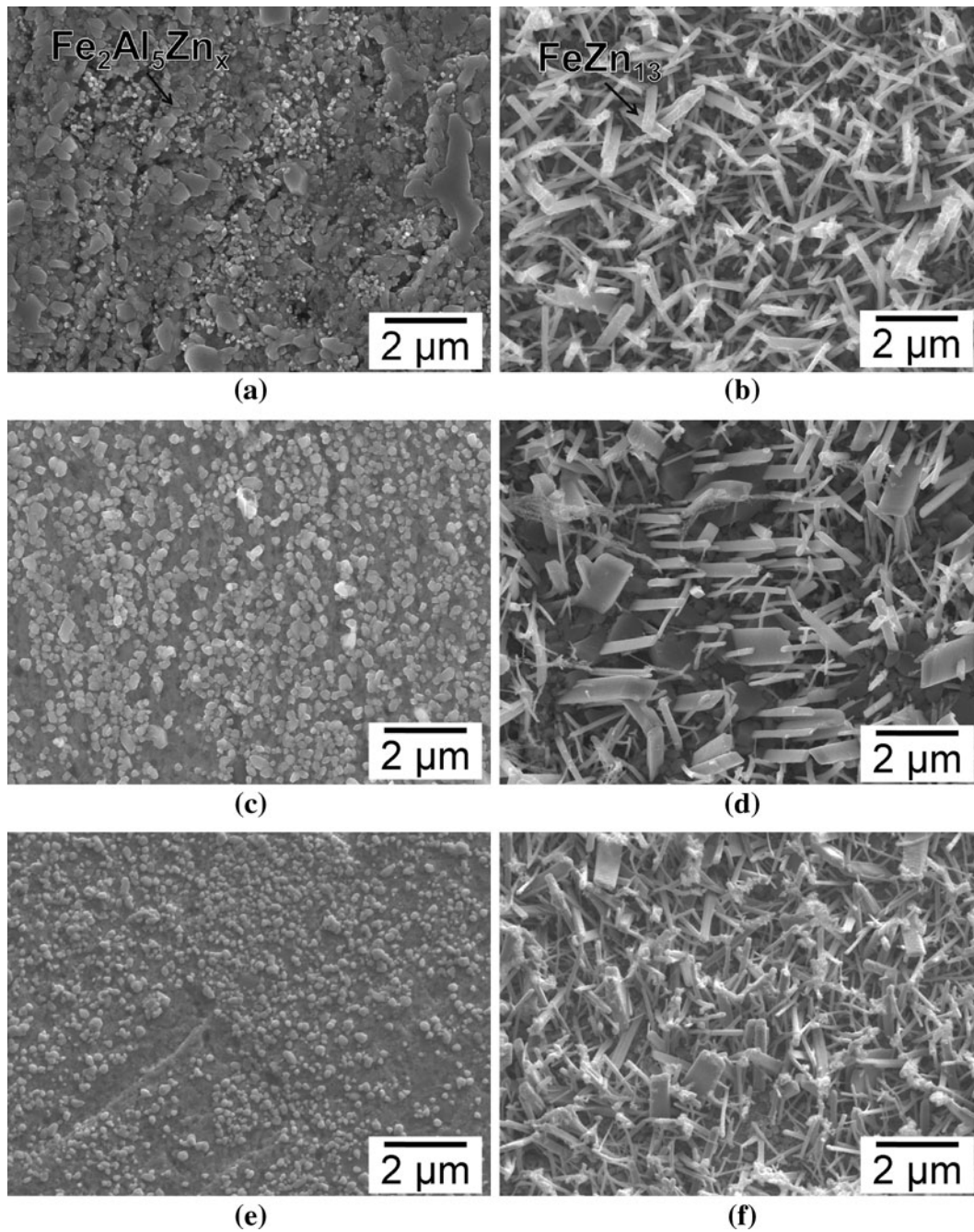
Fig. 10—SEM analysis of the steel/coating interface of (*a*) and (*b*) the 220 K (–53 °C) dp steel, (*c*) and (*d*) the 243 K (–30 °C) dp steel, and (*e*) and (*f*) the 278 K (+5 °C) dp steel. (a), (c) and (e) were stripped with HNO_3, and (b), (d) and (f) were stripped with 10 pct H_2SO_4.

also resulted in internal oxidation of the alloying elements, as shown by TEM analysis of the 278 K (+5 °C) dp steel (Figure 9). Internal oxidation for the 278 K (+5 °C) dp atmosphere has also been observed for other TRIP steel chemistries investigated by the present authors[34,35] and is expected when using higher process atmosphere oxygen partial pressures.[43]

It was determined that the surface and subsurface enrichment behavior of aluminum was different from that of silicon and manganese (Figure 3). This trend was also observed for a steel containing 1.5 pct Al and low Si.[35] The higher concentration of aluminum below the

surface was attributed to the formation of AlN, as observed in Figure 11(a) (point A, Table V). For the 278 K (+5 °C) dp process atmosphere, internal oxidation of aluminum also contributed to the higher aluminum concentration observed below the steel surface (Figure 9).

The oxide morphologies of the 220 K (–53 °C) dp and 243 K (–30 °C) dp samples were similar and comprised a mixture of relatively thin films and nodules (Figures 5 through 7). The surface oxide chemistries of the 220 K (–53 °C) dp and 243 K (–30 °C) dp steels were similar with both steels having a mixture of Mn, Si, and Al rich
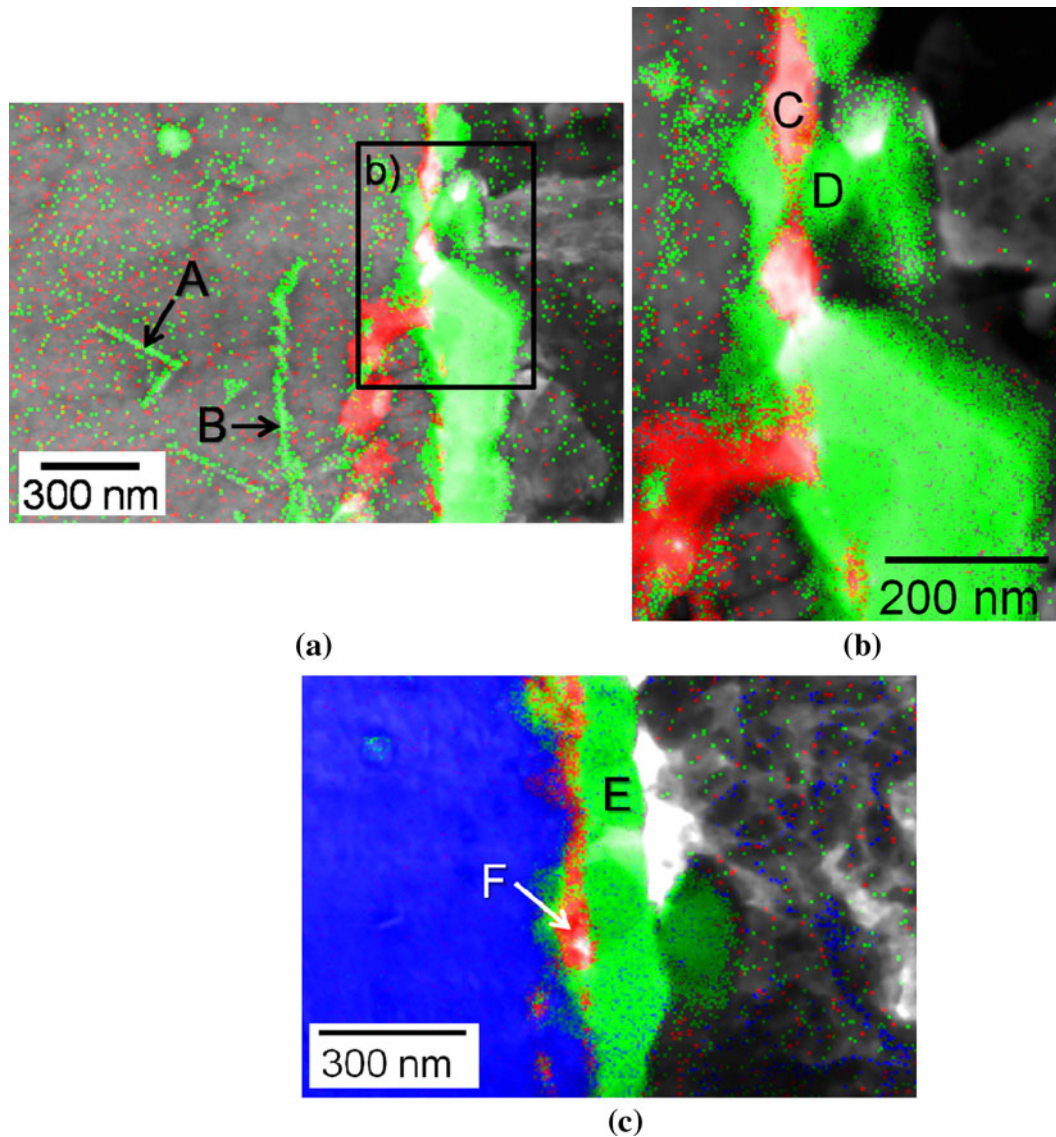
Fig. 11—TEM analysis of the coated 220 K (–53 °C) dp steel: (*a*) STEM bright-field image of area 1; (*b*) STEM bright-field image of area 2, which is an enlargement of the area indicated in (a); and (*c*) STEM bright-field image of area 3. Selected elemental maps are overlaid in color; Mn is shown in red, Al in green, and Fe in blue. The steel substrate is on the left, and the Zn overlay is on the right. Analysis of points A through F is provided in Table V.

Table V. TEM EDX Analysis Corresponding to Points A Through H in Figs. 11 and 12 of the Galvanized 220 K (–53 °C) dp Steel and 278 K (+5 °C) dp Steel, Respectively (Atomic Percent)

Figure	Point	Fe	Zn	Al	Mn	O	Si	N	Phase Present
11	A	67.7	0.1	17.2	0.7	2.1	0.6	11.7	AlN
11	B	46.0	0.1	23.4	0.4	30.0	0.3	—	Al_2O_3
11	C	1.1	0.5	5.9	30.4	49.3	12.9	—	Mn, Al, and Si oxide
11	D	24.5	13.3	58.3	—	3.7	0.2	—	$Fe_2Al_5Zn_x$
11	E	25.4	11.8	57.8	0.1	4.9	—	—	$Fe_2Al_5Zn_x$
11	F	1.6	3.0	9.7	30.7	47.4	7.6	—	Mn, Al, and Si oxide
12	G	11.9	0.3	6.1	25.3	34.9	4.9	—	Mn, Si, and Al oxide
12	H	10.8	0.7	1.8	33.0	37.4	0.5	—	MnO

oxides (Figures 2 through 7 and Table III). It was also observed that the ratio of oxygen to the sum of Mn, Si and Al was consistently too low to be in the MnO-Al_2O_3-SiO_2 system as defined by Jung *et al.*[30,31] (Table III). The oxygen deficiency was attributed to the metallic Mn observed by XPS (Figure 4) and to SiO_x
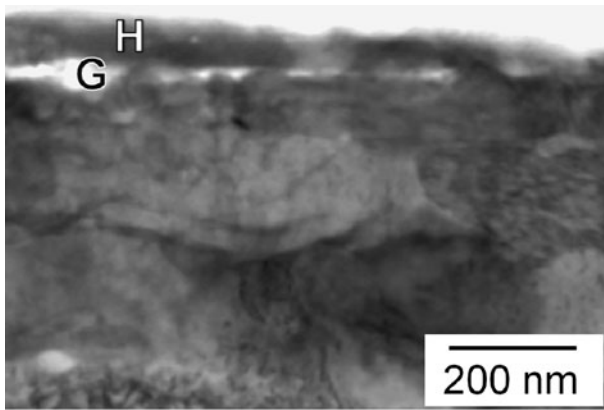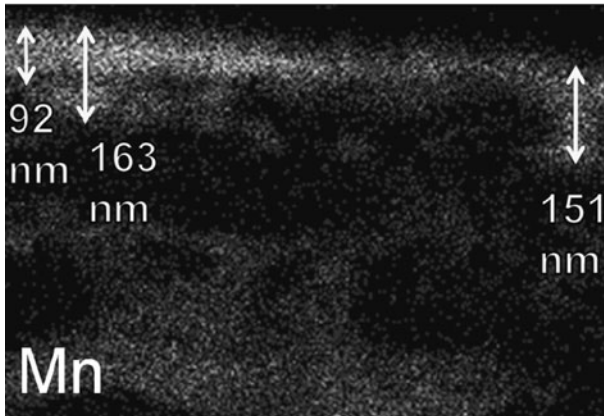
Fig. 12—TEM EDX analysis of the 278 K (+5 °C) dp galvanized steel within a bare spot in the galvanized coating: (*a*) STEM bright field image and (*b*) Mn map. Analysis of points G and H is provided in Table V.

(*x* < 2) identified by TEM EDX analysis (point B in Table III) as well as to the errors associated with oxygen measurement by TEM EDX analysis. Non-stoichiometric SiO_x (*x* < 2) has previously been identified by Van De Putte *et al.*[44] during annealing of a 1.61 pct Mn, 1.45 pct Si steel. The oxides on the steel surface of the 220 K (–53 °C) dp and 243 K (–30 °C) dp steels had a wide range of chemistries as shown by the TEM EDX point analyses (Table III). Similarly, the oxides identified by Gong *et al.*[32] when annealing a Mn, Si and Al containing TRIP steel had a range of chemistries as they were defined as $xMnO \cdot SiO_2$ ($1 \leq x \leq 4$) and $xMnO \cdot Al_2O_3$ ($x \geq 1$).

B. *Reactive Wetting*

Multiple reactive wetting mechanisms were identified for the 220 K (–53 °C) dp and 243 K (–30 °C) dp process atmosphere samples and included aluminothermic reduction, wetting of an oxide film and bridging of oxide particles by the zinc overlay or Fe-Zn intermetallics. Complete reactive wetting was observed for the 220 K (–53 °C) dp and 243 K (–30 °C) dp steels (Table IV) despite almost complete coverage of the surface by film and nodule-type oxides (Figures 2, and 5

through 7). After galvanizing, the 220 K (–53 °C) dp steel no longer had a continuous oxide layer (lower portion of Figures 11(a) and (b)), suggesting chemical removal through reactions with the galvanizing bath. Using the thermodynamic model of McDermid *et al.*,[36] it was previously determined that it is thermodynamically favorable for the dissolved aluminum in the Zn (Al, Fe) bath to reduce a thin MnO film per Eq. [2].[45]
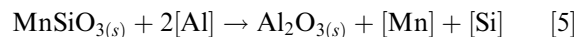
$$3MnO_{(s)} + 2[Al] \xrightarrow{733K(460°C)} Al_2O_{3(s)} + 3[Mn] \quad [2]$$
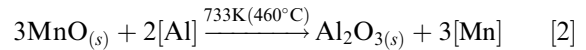
It is also thermodynamically possible for the dissolved aluminum in a 0.2 pct Al bath at 733 K (460 °C) to reduce SiO_2 as shown in the reaction in Eq. [3].

$$3SiO_{2(s)} + 4[Al] \xrightarrow{733K(460°C)} 2Al_2O_{3(s)} + 3[Si] \quad [3]$$
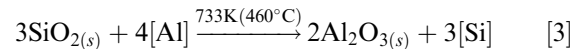
When using a melt silicon activity of 0.0001, which is a high estimate of the silicon activity in the zinc bath, the activity of aluminum in the bath required for equilibrium in Eq. [3] was calculated to be 7.14×10^{-14}.[37,46] The activity of aluminum in the present Zn (Al, Fe) bath was 0.026,[36] many orders of magnitude higher than that required to reduce SiO_2. The activities of SiO_2 and Al_2O_3 were assumed to be one as these are pure condensed species.

Several authors have obtained experimental results which support the occurrence of aluminothermic reduction. Gong *et al.*[47] observed that following galvanizing of a martensitic steel containing 0.15 pct C, 2.0 pct Mn and 0.33 pct Si the $xMnO \cdot SiO_2$ ($1 \leq x < 2$) observed at the steel surface prior to galvanizing was reduced to $MnAl_2O_4$ by the series of reactions shown in Eqs. [4] through [6]. This series of chemical reactions takes into account the range of oxide compositions observed prior to galvanizing.

$$Mn_2SiO_{4(s)} + 2[Al] \rightarrow (MnO)MnSiO_{3(s)} + 2[Al] \quad [4]$$

$$MnSiO_{3(s)} + 2[Al] \rightarrow Al_2O_{3(s)} + [Mn] + [Si] \quad [5]$$

$$Mn_2SiO_{4(s)} + 2[Al] \rightarrow MnAl_2O_{4(s)} + [Mn] + [Si] \quad [6]$$

More recently, Kavitha and McDermid[48] determined the change in MnO film thickness as a function of immersion time in a 733 K (460 °C), 0.2 wt pct dissolved Al galvanizing bath, showing that approximately 90 nm of MnO could be decomposed in 4 seconds. The authors also unambiguously determined the presence of Al_2O_3 at the MnO/Zn alloy interface using electron energy loss spectroscopy (EELS). It was concluded that the aluminothermic reduction of MnO by dissolved aluminum does proceed, although there would appear to be a limit to the amount of MnO which can be decomposed in practical immersion times.

Another wetting mechanism observed for the 220 K (–53 °C) dp and 243 K (–30 °C) dp steels was zinc bridging of oxide particles. It is not necessary for all oxides at the surface to be reduced for complete reactive wetting to occur as $Fe_2Al_5Zn_x$ can form between any

remaining oxides resulting in a continuous zinc layer above these oxides due to surface tension effects. Zinc bridging was observed for larger oxide nodules where $Fe_2Al_5Zn_x$ formed between rather than on top of these oxides, as demonstrated by the Mn and Al maps in Figure 11(b).

Lastly, it was observed that wetting of the oxide could occur. This wetting mechanism was observed for the Mn, Al and Si oxide film indicated by point F in Figure 11(c) and the small Mn-rich nodules indicated by the Mn map in the lower portion of Figures 11(a) and (b). The formation of $Fe_2Al_5Zn_x$ above these oxides is attributed to the size and chemistry of these oxides. $Fe_2Al_5Zn_x$ was able to grow above the small Mn-rich nodules in Figure 11(a) due to the small size of the oxide remaining at the steel/coating interface. $Fe_2Al_5Zn_x$ grew above the oxide film indicated by point F due to the film chemistry. Point F had a higher Mn and Al concentration than Si concentration and it is likely that the low Si concentration allowed for reactive wetting of this oxide film (Table V). It has also been shown by the present authors that bath metal can infiltrate the oxide-substrate interface,[34,35] allowing formation of $Fe_2Al_5Zn_x$ below the oxide (Figure 11).

Incomplete wetting was observed for the 278 K (+5 °C) dp steel, as shown by the increased number of bare spots in the zinc coating (Table IV). The increased number of bare spots was due to the relatively thick localized film-type MnO observed at the steel surface (Figure 12 and Table V). The MnO layer reached a thickness of approximately 160 nm or greater for the 278 K (+5 °C) dp steel whereas the oxide film was approximately 35 to 40 nm thick on the 220 K (–53 °C) dp steel, where complete reactive wetting was observed. The above effect of MnO film thickness on reactive wetting is consistent with the findings of Alibeigi et al.,[49] who have recently determined that the dynamic wetting force for the reactive wetting of a series of manganese containing dual phase steels is inversely proportional to the MnO film thickness, implying the rate limiting step for reactive wetting is the chemical removal of the oxide film. Within the context of the present investigation, the results of Alibeigi et al.[49] imply that the oxide reduction kinetics were not sufficiently rapid to remove the thicker (≥160 nm) MnO layer, but were sufficient to reduce the thinner oxide layers found on the 220 K (–53 °C) dp and 243 K (–30 °C) dp samples (Figures 3, 6, and 12). The kinetic data of Kavitha and McDermid[48] support this conclusion, indicating that for the 4 second immersion times employed in the present study, the 35 to 40 nm thick oxide layer present on the 220 K (–53 °C) dp steel surface (Figure 6) could be aluminothermically reduced (Figure 11), whereas the 160 nm or thicker MnO layer on the 278 K (+5 °C) dp steel surface could not (Figure 12). These findings seem to define a limit to the utility of in situ aluminothermic reduction in aiding the reactive wetting process. It should be pointed out, however, that the localized thick films resulted in localized incomplete reactive wetting as much of the surface of the 278 K (+5 °C) dp steel showed integral coatings. This latter finding combined with the kinetic
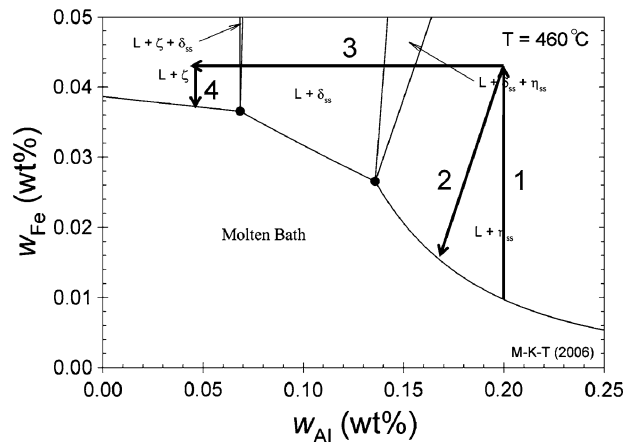

Fig. 13—Zinc rich corner of the Zn-Al-Fe phase diagram[36] with arrows added to indicate processes occurring during galvanizing of the experimental TRIP steel. When the steel is immersed in a 0.2 pct dissolved Al bath iron dissolution from the substrate occurs, as shown by arrow 1. On areas of the steel surface which are free of oxides $Fe_2Al_5Zn_x$ precipitates as shown by arrow 2. At the same time aluminothermic reduction will occur on oxidized areas of the substrate consuming aluminum as indicated by arrow 3. If aluminum is not replenished Fe-Zn intermetallics will precipitate, as shown by arrow 4.

information of Kavitha and McDermid[48] correlates well with the observations of Figure 9, where it was shown that there were MnO films up to 90 nm thick on the 278 K (+5 °C) dp sample surface, which could be aluminothermically reduced in the 4 second immersion time.

$FeZn_{13}$ was observed at the steel/coating interface for all process atmospheres. The presence of $FeZn_{13}$ was not expected when galvanizing using a 0.2 pct dissolved Al bath. Full inhibition (i.e., the formation of a continuous $Fe_2Al_5Zn_x$ layer without the presence of $FeZn_{13}$) is expected when the bath Al content is greater than 0.15 pct.[51] The majority of $FeZn_{13}$ identified on these steels was not associated with inhibition breakdown, where $FeZn_{13}$ formed on or between $Fe_2Al_5Zn_x$ grains rather than as outbursts. The presence of $FeZn_{13}$ in this morphology could indicate a localized depletion of aluminum in the bath due to the combined effects of oxide reduction reactions and the formation of $Fe_2Al_5Zn_x$. In the present case, $FeZn_{13}$ formation arose from the combination of aluminum depletion at the substrate coating interface and continued mass transport of iron through the $Fe_2Al_5Zn_x$ layer prior to coating solidification.[41,50] This process is schematically illustrated in Figure 13. In this case, it is assumed that the iron content adjacent to the substrate is quite high, as would be expected from the dissolution reaction.

V. CONCLUSIONS

Selective oxidation and galvanizing was studied for a TRIP-assisted steel with 1.5 pct Mn, 1.0 pct Al and 0.5 pct Si as a function of oxygen partial pressure of the process atmosphere. For the 220 K (–53 °C) dp and 243 K (–30 °C) dp process atmospheres the surface was

almost completely covered with Mn, Si, and Al rich oxides. The morphology of these oxides comprised both nodules and relatively thin films. Despite significant coverage of the surface by these oxides complete reactive wetting was observed. Complete wetting was attributed to the oxide chemistry, thickness and morphology. The oxide chemistry and thickness made it possible for aluminothermic reduction to occur, allowing bath metal to come in contact with the substrate to form the desired $Fe_2Al_5Zn_x$ interfacial layer. $Fe_2Al_5Zn_x$ formed between, above or below oxides not chemically removed from the substrate surface during galvanizing, allowing bridging of oxides by the zinc overlay.

There was an increase in the number of bare spots and percentage bare area in the zinc overlay when using the 278 K ($+5$ °C) dp process atmosphere. The incomplete wetting observed for the 278 K ($+5$ °C) dp atmosphere was attributed to relatively thick, localized film-type MnO observed at the surface, indicating that aluminothermic reduction kinetics were insufficient to reduce the 160 nm MnO films during a 4 second immersion in the Zn (Al, Fe) bath.

$FeZn_{13}$ was identified at the steel/coating interface of all samples. The presence of $FeZn_{13}$ was associated with consumption of aluminum in the mass transport boundary layer *via* aluminothermic reduction and formation of $Fe_2Al_5Zn_x$.

REFERENCES

1. M. Takahashi, H. Yoshida, and S. Hiwatashi: *Int. Conf. on TRIP-Aided High Strength Ferrous Alloys*, Ghent, Belgium, June 19–21, 2002, pp. 103–11.
2. J. Van Slycken, P. Verleysen, J. Degrieckm, J. Bouquerel, and B.C. De Cooman: *Mater. Sci. Eng. A*, 2007, vols. 460–461, pp. 516–24.
3. B.C. De Cooman: *Curr. Opin. Solid State Mater. Sci.*, 2004, vol. 8, pp. 285–303.
4. P. Jacques, X. Cornet, P. Harlet, J. Ladrière, and F. Delannay: *Metall. Mater. Trans. A*, 1998, vol. 29A, pp. 2383–93.
5. O. Matsumura, Y. Sakuma, and H. Takechi: *Trans. ISIJ*, 1987, vol. 27, pp. 570–79.
6. Y. Tomota, H. Tokuda, Y. Adachi, M. Wakita, A. Moriai, and Y. Morii: *Acta Mater.*, 2004, vol. 52, pp. 5737–45.
7. P. Jacques, Q. Furnémont, A. Mertens, and F. Delannay: *Phil. Mag. A*, 2001, vol. 81, pp. 1789–1812.
8. P.J. Jacques, E. Girault, A. Mertens, B. Verlinden, J. Van Humbeeck, and F. Delannay: *ISIJ Int.*, 2001, vol. 41, pp. 1068–74.
9. E. Girault, A. Mertens, P. Jacques, Y. Houbaert, B. Verlinden, and J. Van Humbeeck: *Scripta Mater.*, 2001, vol. 44, pp. 885–92.
10. A.K. Srivastava, D. Battacharjee, G. Jha, N. Gope, and S.B. Singh: *Mater. Sci. Eng. A*, 2007, vols. 445–446, pp. 549–57.
11. A.N. Vasilakos, J. Ohlert, K. Giasla, G.N. Haidemenopoulos, and W. Bleck: *Steel Res.*, 2002, vol. 73, pp. 249–52.
12. M. De Meyer, D. Vanderschueren, and B.C. De Cooman: *ISIJ Int.*, 1999, vol. 39, pp. 813–22.
13. J. Mahieu, J. Maki, B.C. De Cooman, and S. Claessens: *Metall. Mater. Trans. A*, 2002, vol. 33A, pp. 2573–80.
14. H.C. Chen, H. Era, and M. Shimizu: *Metall. Trans. A*, 1989, vol. 20A, pp. 437–45.
15. A. Pichler, S. Traint, G. Arnolder, P. Stiaszny, M. Blaimschein, and E.A. Werner: *Iron Steelmaker*, 2003, vol. 30, pp. 21–31.
16. J. McDermid, S. Dionne, O. Dremailova, B. Voyzelle, E. Essadiqi, E. Baril, and F. Goodwin: *2005 SAE World Congress*, Society for Automotive Engineers, Detroit, MI, 2005, paper no. 2005-01-0495.
17. S.C. Baik, S. Kim, Y.S. Jin, and O. Kwon: *ISIJ Int.*, 2001, vol. 41, pp. 290–97.
18. H. Matsuda, F. Kitano, K. Hasegawa, T. Urabe, and Y. Hosoya: *Steel Res.*, 2002, vol. 73, pp. 211–17.
19. D. Krizan, B.C. De Cooman, and J. Antonissen: *Int. Conf. Adv. High Strength Sheet Steels Autom. Appl. Proc.*, AIST, Warrendale, PA, 2004, pp. 205–16.
20. A. Mertens and J. McDermid: *Mater. Sci. Technol. 2005*, Pittsburgh, PA, Sept. 25–28, 2005, pp. 199–210.
21. A. Mertens and J.R. McDermid: *Materials Science and Technology (MS&T) 2006: Materials and Systems–Volume 2*, Cincinnati, OH, Oct. 15–19, 2006, pp. 131–42.
22. E.M. Bellhouse and J.R. McDermid: *Metall. Mater. Trans. A*, 2010, vol. 41A, pp. 1460–73.
23. P. Drillet, Z. Zermout, D. Bouleau, J. Mataigne, and S. Claessens: *Proc. 6th Int. Conf. on Zinc Alloy Coated Steel Sheet–Galvatech 2004*, Chicago, IL, Apr. 4–7, 2004, Association for Iron and Steel Technology, Warrendale, PA, 2004, pp. 1123–34.
24. J. Mahieu, B.C. De Cooman, J. Maki, and S. Claessens: *Iron Steelmaker*, 2002, vol. 29, pp. 29–34.
25. M.S. Kim, J.H. Kwak, J.S. Kim, Y.H. Liu, N. Gao, and N.-Y. Tang: *Metall. Mater. Trans. A*, 2009, vol. 40A, pp. 1903–10.
26. J. Mahieu, S. Claessens, and B.C. De Cooman: *Metall. Mater. Trans. A*, 2001, vol. 32A, pp. 2905–08.
27. J. Maki, J. Mahieu, B.C. De Cooman, and S. Claessens: *Mater. Sci. Technol.*, 2003, vol. 19, pp. 125–31.
28. J. Mahieu, S. Classens, B.C. De Cooman, and F. Goodwin: *Proc. 6th Int. Conf. on Zinc Alloy Coated Steel Sheet–Galvatech 2004*, Chicago, IL, Apr. 4–7, 2004, Association for Iron and Steel Technology, Galvatech, pp. 529–38.
29. F.B. Pickering: *Physical Metallurgy and the Design of Steels*, Applied Science Publishers Ltd, London, 1978, p. 11.
30. I.-H. Jung, Y.-B. Kang, S.A. Decterov, and A.D. Pelton: *Metall. Mater. Trans. B*, 2004, vol. 35B, pp. 259–68.
31. I.-H. Jung, M. Paliwal, Y.-M. Kim, S.-K. Lee, and J.-S. Kim: *Proc. Asia-Pacific Galvanizing Conf.*, Jeju, Korea, Nov. 8–12, 2009, The Corrosion Science Society of Korea, Seoul, paper no. A-34.
32. Y.F. Gong, Y.R. Lee, H.S. Kim, and B.C. De Cooman: *Proc. Asia-Pacific Galvanizing Conf.*, Nov. 8–12, 2009, Jeju, Korea, The Corrosion Science Society of Korea, Seoul, paper no. A-41.
33. X.S. Li, S.-I. Baek, C.-S. Oh, S.-J. Kim, and Y.-W. Kim: *Scripta Mater.*, 2008, vol. 59, pp. 290–93.
34. E.M. Bellhouse and J.R. McDermid: *Metall. Mater. Trans. A*, 2010, vol. 41A, pp. 1539–53.
35. E.M. Bellhouse and J.R. McDermid: *Metall. Mater. Trans. A*, 2011, vol. 42A, pp. 2753–68.
36. J.R. McDermid, M.H. Kaye, and W.T. Thompson: *Metall. Mater. Trans. B*, 2007, vol. 38B, pp. 215–30.
37. H.A. Fine and G.H. Geiger: *Handbook on Material and Energy Balance Calculations in Metallurgical Processes*, TMS-AIME, Warrendale, PA, 1979, pp. 385 and 428.
38. B.R. Strohmeier and D.M. Hercules: *J. Phys. Chem.*, 1984, vol. 88, pp. 4922–29.
39. M.C. Biesinger, B.P. Payne, A.P. Grosvenor, L.W.M. Lau, A.R. Gerson, and R.St.C. Smart: *Appl. Surf. Sci.*, 2011, vol. 257, pp. 2717–30.

40. E. Baril and G. L'Esperance: *Metall. Mater. Trans. A*, 1999, vol. 30A, pp. 681–95.
41. L. Chen, R. Fourmentin, and J.R. McDermid: *Metall. Mater. Trans. A*, 2008, vol. 39A, pp. 2128–42.
42. T. Nakamori, Y. Adachi, T. Toki, and A. Shibuya: *ISIJ Int.*, 1996, vol. 36, pp. 179–86.
43. H.J. Grabke, V. Leroy, and H. Viefhaus: *ISIJ Int.*, 1995, vol. 35, pp. 95–113.
44. T. Van De Putte, D. Loison, J. Penning, and S. Claessens: *Metall. Mater. Trans. A*, 2008, vol. 39A, pp. 2875–84.
45. R. Khondker, A. Mertens, and J.R. McDermid: *Mater. Sci. Eng. A*, 2007, vol. 463, pp. 157–65.
46. O. Kubaschewski and C.B. Alcock: *Metallurgical Thermochemistry*, 5th ed., Pergamon Press, Oxford, United Kingdom, 1979, p. 382.
47. Y.F. Gong, T.J. Song, H.S. Kim, J.H. Kwak, and B.C. DeCooman: *Proc. Asia-Pacific Galvanizing Conf. 2009*, Jeju, Korea, Nov. 8–12, 2009, The Corrosion Science Society of Korea, Seoul, Korea, paper no. B-15.
48. R. Kavitha and J.R. McDermid: *Proc. 8th Int. Conf. on Zinc Alloy Coated Steel Sheet–Galvatech 2011: Steel Surface Characterization*, Genova, Italy, June 21–24, 2011, Associazione Italiana di Metallurgia, Milan, Italy, 2011.
49. S. Alibeigi, R. Kavitha, R.J. Meguerian, and J.R. McDermid: *Acta Mater.*, 2011, vol. 59, pp. 3537–49.
50. P. Toussaint, L. Segers, R. Winand, and M. Dubois: *ISIJ Int.*, 1998, vol. 38, pp. 985–90.
51. N.-Y. Tang: *Zinc-Based Steel Coating Systems: Production and Performance*, TMS, Warrendale, PA, 1998, pp. 3–12.